Thermoelectric transport properties of molybdenum from abinitio simulations

Martin French and Thomas R. Mattsson

Phys. Rev. B **90**, 165113 — Published 10 October 2014

DOI: 10.1103/PhysRevB.90.165113

Thermoelectric transport properties of molybdenum from *ab initio* simulations

Martin French and Thomas R. Mattsson
HEDP Theory, Sandia National Laboratories, Albuquerque, New Mexico 87185-1189, USA
(Dated: September 19, 2014)

We employ *ab initio* simulations based on density functional theory (DFT) to calculate the electronic transport coefficients (electrical conductivity, thermal conductivity, and thermopower) of molybdenum over a broad range of thermodynamic states. By comparing to available experimental data, we show that DFT is able to describe the desired transport properties of this refractory metal with high accuracy. Most noteworthy, both the positive sign and the quantitative values of the thermopower of solid molybdenum are reproduced very well. We calculate the electrical and thermal conductivity in the solid and the fluid phase between 1000 K and 20 000 K and a wide span in density and develop empirical fit formulae for direct use in practical applications, such as magneto-hydrodynamics simulations. The influence of thermal expansion in conductivity measurements at constant pressure is also discussed in some detail.

PACS numbers: 31.15.A-, 72.15.Jf, 52.25.Fi

I. INTRODUCTION

Refractory metals like molybdenum are technologically important materials because of their high mechanical strength, high melting point, supreme resistance to heat and corrosion, as well as good electrical conductivity.[1] Molybdenum is commonly used in high-strength steels as well as superalloys for applications in extreme environments like turbine blades in jet engines and for components in gas turbines. A new application for molybdenum, involving even more extreme conditions in pressure and temperature, is as a drive material in pulsed-power experiments aiming to measure high-pressure yield strenghts of sample materials under shear stress (MAPS).[2] Understanding the physical processes involved as well as designing and optimizing the experiments rely on the use of magneto-hydrodynamic (MHD) simulations. The MHD simulations, in turn, rely on using accurate material models like equation of state (EOS) in general and thermoelectric transport coefficients in particular. Errors in the electrical conductivity model can lead, for example, to incorrect joule heating in the simulations, driving the simulations away from the correct thermodynamic state as the simulation evolves in time. There is therefore a need to have an accurate model for the thermoelectric properties of molybdenum over a broad range of conditions, including the transition from solid state behavior to dense plasma, the warm dense matter region, a part of the phase diagram which is challenging to describe.

Molybdenum is a bcc metal and, like many of the transition metals, it has a complex electronic structure. Three examples of effects due to the involved electronic structure are the positive signs of the thermopower[3] and Hall coefficient[4] near ambient conditions and the anomalous self-diffusion behavior at high temperature below the melting point.[5] The electrical conductivity, σ, in solid molybdenum is accurately known up to the melting point[6] at ambient pressure. It was also measured in the liquid phase[7–10] and in plasma states[11] using exploding wire experiments. The thermal conductivity, λ, of solid molybdenum was probed experimentally up to melting.[12–18] In the liquid it is typically approximated from the electrical conductivity using the Wiedemann-Franz law.[19]

In this paper, we present results from extensive *ab initio* calculations for the thermoelectric transport coefficients of molybdenum that are based on finite-temperature density functional theory (FT-DFT).[20–22] Within this framework the electronic transport coefficients are derived with expressions obtained from Linear Response Theory (LRT).[23] Although σ and λ are the quantities of primary practical importance, we also examine the thermopower α in some detail. This quantity does not depend directly on the concentration of free charge carriers (here best described as conduction electrons) and is very sensitive to the electronic structure. By reproducing the experimental thermopower in the solid, in addition to the conductivities in various phases, we ensure that our calculated results are of very high fidelity.

Transport properties often change significantly when phase boundaries are crossed. It is therefore important to know the location of the melt boundary. Explicit calculations of the melt boundary are not performed here, however, because of the extensive previous experimental[24–28] and theoretical[29–35] work regarding the phase diagram of molybdenum. All thermodynamic conditions of interest here (1000 K to 20 000 K and up to 2 Mbar) are either in the fluid or in the bcc solid, and we thus calculate the transport properties for these two phases.

Following this introduction is a section on the theoretical methods used, a section presenting results and extensive comparisons with available experimental data, and finally a summary and discussion. We expect the results in the article to be used to model molybdenum

under high pressure and high temperature and to serve as an example on how one can approach systematic modeling of thermoelectric transport properties of materials with challenging electronic structure.

II. THEORY AND SIMULATION DETAILS

Our theoretical approach to calculate the electronic transport coefficients relies on performing FT-DFT molecular dynamics (MD) simulations in the Born-Oppenheimer approximation to obtain thermophysical properties like internal energy and pressure and an ensemble of ionic configurations at each thermodynamic state. Subsequently, static FT-DFT calculations are done for each of the ionic configurations to evaluate the LRT expressions for thermoelectrical properties. This has become a well established procedure for electronic transport calculations over the last ten years. It has been successfully applied for various materials, mostly with focus on the electrical conductivity.[23,36–41] In this paper, in addition to conductivity, we also calculate the thermal transport properties, thus making full use of the theoretical approach. The Vienna *ab initio* simulation package (VASP) 5.3.2,[42–46] which is a plane-wave pseudopotential code, is used for both the MD simulations and transport calculations.

The calculation of the thermoelectric transport coefficients is based on the following expressions for the Onsager coefficients derived within LRT:[23]

$$L_{mn}(\omega) = \frac{2\pi(-e)^{4-m-n}}{3\Omega\omega} \sum_{\mathbf{k}\nu\mu} |\langle \mathbf{k}\nu|\hat{\mathbf{v}}|\mathbf{k}\mu\rangle|^2 (f_{\mathbf{k}\nu} - f_{\mathbf{k}\mu}) \times \left(\frac{E_{\mathbf{k}\mu} + E_{\mathbf{k}\nu}}{2} - h_e\right)^{m+n-2} \delta(E_{\mathbf{k}\mu} - E_{\mathbf{k}\nu} - \hbar\omega)\,, \quad (1)$$

where ω is the frequency, Ω the volume of the simulation box, e the elementary charge, h_e the enthalpy per electron, $E_{\mathbf{k}\mu}$ and $f_{\mathbf{k}\mu}$ are the eigenvalue and Fermi occupation number of the Bloch state $|\mathbf{k}\mu\rangle$, and $\langle \mathbf{k}\nu|\hat{\mathbf{v}}|\mathbf{k}\mu\rangle$ are matrix elements with the velocity operator.[47] A Gaussian function is used to slightly broaden the delta function to a finite width as necessary.

The static electrical conductivity is directly given by the coefficient $L_{11}(\omega)$, also known as the Kubo-Greenwood formula,[48,49] in the limit of zero frequency:

$$\sigma = \lim_{\omega\to 0} L_{11}(\omega). \quad (2)$$

Second, the thermal conductivity is calculated via the relation:

$$\lambda = \lim_{\omega\to 0} \frac{1}{T}\left(L_{22}(\omega) - \frac{L_{12}^2(\omega)}{L_{11}(\omega)}\right). \quad (3)$$

The thermopower is defined as

$$\alpha = \lim_{\omega\to 0} \frac{L_{12}(\omega)}{T L_{11}(\omega)}. \quad (4)$$

The zero-frequency limits are taken by making linear fits to the results from the above expressions in a narrow frequency interval, excluding the abrupt and unphysical decrase to zero in the $L_{mn}(\omega = 0)$ which occurs due to the finite number of particles in the calculations. The width of this interval is selected as narrow as possible, and it is usually different for each of the individual transport coefficients (2), (3), and (4) because of their different frequency behaviors. It also depends on density, temperature, and particle number and thus the procedure needs to be performed manually for each particular calculation.

The most important aspect of DFT calculations is the choice of exchange-correlation functional. For Mo, the AM05 exchange-correlation functional[50,51] gives very good equilibrium density and bulk modulus[5] and was therefore used in all calculations above 4 g/cm^3. For expanded states, we used the PBE functional[52] instead since PBE gives good atomization energies, a property that is important in the region around the critical point. Furthermore, calculations for expanded states converge significantly better with PBE than with AM05.[53] We verified that AM05 and PBE yield identical results for the thermoelectric transport properties in test calculations of several states above 4 g/cm^3.

Of particular importance is the fidelity of the pseudopotentials employed to reduce the number of electrons carried self-consistently in the FT-DFT calculations.[54] We exclusively use the GW-labeled 14 electron projector-augmented wave (PAW) pseudopotential[55,56] in all LRT calculations (with 300 eV cutoff energy) and in all MD simulations of the fluid (with 800 eV cutoff energy). In a recent technical report,[57] it was shown that various other molybdenum pseudopotentials for VASP produce slightly less accurate results for the lattice constant and electronic density of states, even in ground-state calculations. During the construction of the GW-labeled set of pseudopotentials, special care was taken with the projectors for the (at zero temperature) unoccupied Kohn-Sham states.[56] These states become relevant when they are partially occupied at high temperatures[54] or when involved in calculating transition matrix elements.

The high accuracy of the 14 electron potential notwithstanding, the 6 electron PAW potential (with 400 eV cutoff energy) was used in the MD simulations to create the ensemble of ionic configurations of the solid, where the thermal occupation of excited states is still small. In test calculations we checked that using either of the two PAW potentials in these MD simulations did not influence the electronic transport coefficients. Importantly, the subsequent LRT calculations of thermoelectric properties were all done using the 14 electron GW-labeled PAW potential.

Achieving sound numerical convergence is a fundamental aspect in FT-DFT.[58] Depending on the phase of the system, i.e., fluid or solid, different numerical parameters were used. The relevant settings, especially the particle number and the **k**-point grids, were extensively convergence tested.

All MD simulations were made in the canonical ensemble (NVT) using a Nosé thermostat[59] and the Baldereschi **k**-point.[60] Following equilibration, each thermodynamic state was run for 3000 to 20 000 time steps of length of 1 to 4 fs, depending on temperature using a velocity-verlet time integration algorithm.

In the fluid phase, excellent convergence of all transport coefficients could be achieved with 54 atoms at or above 5 g/cm^3 and with 24 atoms at lower densities. The respective LRT calculations (using 25-40 ionic configurations from each MD) were done with a standard $2 \times 2 \times 2$ Monkhorst-Pack grid.[61] Table I contains two representative examples of convergence tests made for the fluid phase.

Calculating converged thermoelectric transport coefficients for the solid is much more demanding than for the fluid, especially at low temperatures. The long mean free path of the electrons requires both larger simulation boxes (with more particles) as well as denser **k**-point meshes due to the high symmetry of the ionic configurations. We illustrate this with two examples in Table I. Increasing the particle number and **k**-point grids does not necessarily lead to a uniform convergence of the transport coefficients and outliers may occur. Furthermore, full convergence of σ, λ, and α can be achieved with different simulation parameters for each of them, whereas α usually involves the lowest and λ the highest numerical effort. For instance, at 1000 K one can calculate a well-converged thermopower with 128 atoms, while the electrical conductivity requires at least 250 atoms. The thermal conductivity can be determined barely within a few percent at 1000 K, but this improves rapidly at higher temperature. Our second example at 2500 K shows that the higher thermal disorder in the lattice leads to a much better convergence for all transport coefficients.

As a consequence, we made extensive sets of calculations with 54, 128, and 250 atoms using different **k**-point sets for each considered density and temperature below 3000 K. All final results for the transport coefficients in the solid phase were taken from the MD simulations with 250 atoms. An irreducible wedge of the $4 \times 4 \times 4$ **k**-point grid was used in the respective LRT calculations. This generally produced very well converged results for all transport coefficients. The occasional tendency toward an underestimation of the thermal conductivity at 1000 K did not affect the quality of the fit function derived from the complete set of results, Eq. (8).

To conclude on the methodology for calculating thermoelectric properties, we did not calculate the contribution of the phonons to the thermal conductivity of the solid. The reason is that the Wiedemann-Franz law is fulfilled within a few percent at room temperature,[1,6] see subsection III C. Therefore the ionic contribution is likely to be very small and it further decreases, usually with $1/T$ behavior at elevated temperatures above the Debye temperature.[62] The phonon contribution to the thermal conductivity therefore does not need to be taken into account at the high temperatures that is the focus of the present work.

III. RESULTS

Here we present the results for the thermoelectric transport properties and compare with available experiments. We note that the FT-DFT-MD simulations also yield the equation of state as a byproduct, with which we can estimate the critical density of molybdenum to be near 3 g/cm^3 and the critical temperature near 11 000 K. This result is close to earlier estimations from theory and experiment.[63–65] Our main data set ranges across a regular grid from 2 to 13 g/cm^3 and from 1000 to 20 000 K, excluding the thermodynamically unstable region in the subcritical fluid.

In some cases the finite number of atoms in our MD boxes allowed us to simulate both a liquid and solid phase at identical density and temperature. Having such an overlap of results is very helpful for our purposes. It significantly reduces the need to extrapolate the fit formulae when approaching the melting line.

A. Electrical conductivity

We display several isochores of the electrical conductivity in Fig. 1. In both the liquid and solid phases the electrical conductivity increases roughly linearly with the density. The temperature dependence, however, is drastically different between the liquid and solid phase. While the conductivity decreases strongly with the temperature in the solid, it is almost independent of temperature in the liquid up to about 10 000 K. This is a relatively common behavior for a metallic system[6,66] and is a consequence of the drastic change in the electronic and ionic structure at melting. At higher temperatures the electrical conductivity shows a linear temperature dependence. It decreases if the density is sufficiently high but increases at lower densities, which is a well-known property of expanded metallic liquids and plasmas. This inversion of the temperature behavior occurs near 4 g/cm^3.

The following simple expression was found to lead to an excellent fit for the electrical conductivities in the solid, σ_s. It reads:

$$T\sigma_s = a_0 + a_1\varrho + a_2 T + a_3 \ln T \tag{5}$$

The coefficients a_i are given in Table II. Before performing the least-squares fit, we combined our calculated conductivity results set, which does not include any data below 1000 K, with the accepted experimental data[6] between 250 K and 1000 K. The fit formula is thus applicable from room temperature up to the melt line for densities between 9 and 13 g/cm^3. The volume expansion has been taken into account when processing the experimental data, see Appendix A for details. The resulting fit curves are included in Fig. 1.

TABLE I. Representative convergence tests for the calculated thermoelectric properties with respect to the number of atoms N and the Monkhorst-Pack **k**-point meshes[61] used in the LRT calculations. The thermodynamic states are located in the dense and expanded fluid at 10 000 K and in the solid at 1000 K and 2500 K. The RW indicates that a reduced wedge of the **k**-point grid is used, generated by projection of the full grid into the irreducible Brillouin zone of an ideal bcc lattice. Especially, the RW $2 \times 2 \times 2$ corresponds to the Baldereschi mean-value point.[60]

T (K)	ϱ (g/cm^3)	N	**k** points	σ (MS/m)	λ (W/Km)	α (μV/K)
10 000	5	24	Γ	0.50 ± 0.02	85 ± 3	6 ± 4
10 000	5	24	$2 \times 2 \times 2$	0.47 ± 0.01	91 ± 1	4 ± 2
10 000	5	24	$3 \times 3 \times 3$	0.47 ± 0.01	90 ± 1	3 ± 2
10 000	5	54	Γ	0.46 ± 0.01	93 ± 2	3 ± 3
10 000	5	54	$2 \times 2 \times 2$	0.46 ± 0.01	90 ± 1	3 ± 2
10 000	13	54	Γ	1.53 ± 0.02	334 ± 6	17 ± 4
10 000	13	54	$2 \times 2 \times 2$	1.49 ± 0.01	343 ± 2	13 ± 2
10 000	13	54	$3 \times 3 \times 3$	1.48 ± 0.01	342 ± 2	14 ± 2
10 000	13	128	Γ	1.49 ± 0.01	343 ± 2	12 ± 3
10 000	13	128	$2 \times 2 \times 2$	1.50 ± 0.01	344 ± 2	14 ± 2
1000	10	54	RW $4 \times 4 \times 4$	3.6 ± 0.4	68 ± 7	40 ± 10
1000	10	54	RW $6 \times 6 \times 6$	3.2 ± 0.3	68 ± 5	14 ± 6
1000	10	54	RW $8 \times 8 \times 8$	3.2 ± 0.3	72 ± 5	16 ± 5
1000	10	128	RW $2 \times 2 \times 2$	4.6 ± 0.4	89 ± 6	4 ± 8
1000	10	128	RW $4 \times 4 \times 4$	3.6 ± 0.2	83 ± 5	21 ± 6
1000	10	128	RW $6 \times 6 \times 6$	3.5 ± 0.1	79 ± 4	16 ± 5
1000	10	128	RW $8 \times 8 \times 8$	3.5 ± 0.1	83 ± 4	17 ± 5
1000	10	250	RW $2 \times 2 \times 2$	4.3 ± 0.2	84 ± 5	8 ± 7
1000	10	250	RW $4 \times 4 \times 4$	4.0 ± 0.1	91 ± 4	16 ± 6
1000	10	250	RW $6 \times 6 \times 6$	4.0 ± 0.1	90 ± 4	19 ± 5
1000	10	432	RW $2 \times 2 \times 2$	4.0 ± 0.1	83 ± 5	50 ± 10
2500	13	54	RW $6 \times 6 \times 6$	2.9 ± 0.2	176 ± 7	5 ± 5
2500	13	54	RW $8 \times 8 \times 8$	2.9 ± 0.2	175 ± 6	5 ± 5
2500	13	128	RW $4 \times 4 \times 4$	3.0 ± 0.1	171 ± 5	14 ± 5
2500	13	128	RW $6 \times 6 \times 6$	2.9 ± 0.1	173 ± 5	12 ± 5
2500	13	250	RW $2 \times 2 \times 2$	3.2 ± 0.2	172 ± 6	19 ± 6
2500	13	250	RW $4 \times 4 \times 4$	3.0 ± 0.1	177 ± 4	14 ± 5

TABLE II. Coefficients for the electrical σ_s (second row) and thermal conductivity λ_s (third row) of solid molybdenum. All units are chosen in a way that entering temperatures in K and densities in g/cm^3 leads to results in MS/m for σ_s or W/Km for λ_s, respectively.

	$T\sigma_s$	λ_s
a_0	1514	96.8
a_1	1204	30.4
a_2	0.796	0.0237
a_3	-1506	-47.7

Finding a closed fit formula for the electrical conductivity in the fluid phase is difficult. For simplicity, we split the expression into a temperature-independent part valid in the subcritical liquid and a part with linear temperature dependence for higher temperatures. All values in the liquid up to 8000 K can be fitted very accurately with the simple formula:

$$\sigma_{f1} = b_0 + b_1 \varrho \tag{6}$$

The remaining results (between 10 000 K and 20 000 K) were used to parametrize the expression:

$$\sigma_{f2} = b_0 + b_1 \varrho + b_2 \varrho^2 + b_3 T + b_4 \varrho T + b_5 \varrho^2 T \tag{7}$$

It is very easy to make a steady connection between the above formulae. The coefficients b_i for the Equations (6) and (7) are collected in Table III. Fig. 1 shows how the resulting fit curves match the *ab inito* results.

A comparison of our conductivities with experiments is shown in Fig. 2, which displays the electrical resistivity $R = 1/\sigma$. For the solid we find very good agreement with the values recommended by Desai *et al.*[6] and with the data from Hixson & Winkler.[9] The thermal expansion of the solid has been taken into account, see Appendix A.

The electrical resistivity of liquid molybdenum has been measured in exploding wire experiments.[7–10] The

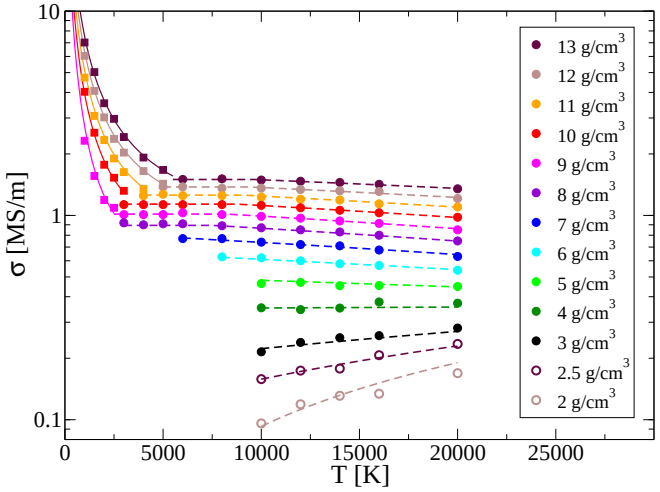

FIG. 1. (Color online) Isochores of the electrical conductivity of molybdenum. For the fluid phase the calculated values are shown as circles, whereas squares of identical color indicate results in the solid phase. The solid lines are results of Eq. (5). The dashed lines correspond to a steady connection of the Equations (6) and (7) for the fluid phase, respectively.

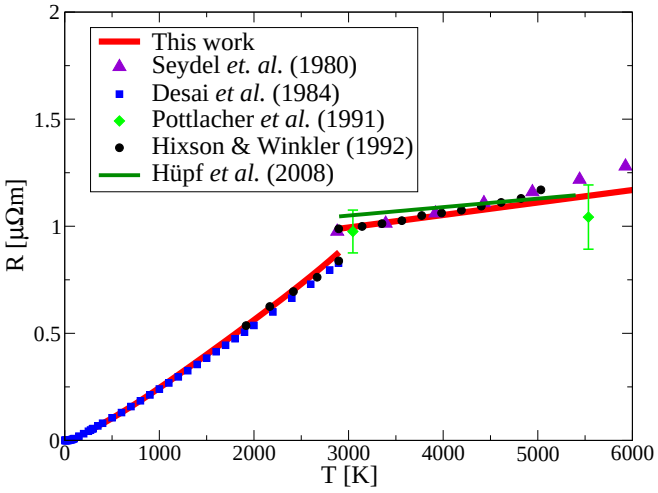

FIG. 2. (Color online) Electrical resistivity of molybdenum from Eq. (5) and (6) in comparison with experiments.[6–10] The resistivity increases abruptly at the melt boundary (2900 K). The experiments were performed at ambient pressure. The volume expansion for the solid was calculated as described in the Appendix A. The expansion data from Hüpf *et al.*[10] was used for the liquid.

TABLE III. Coefficients for the electrical conductivities σ_{f1} (second row) and σ_{f2} (third row) of fluid molybdenum. All units are chosen in a way that entering temperatures in K and densities in g/cm^3 leads to results in MS/m.

	σ_{f1}	σ_{f2}
b_0	-0.074	-0.383
b_1	0.121	0.195
b_2	-	-3.09×10^{-3}
b_3	-	2.14×10^{-5}
b_4	-	-6.39×10^{-6}
b_5	-	2.83×10^{-7}

agreement of our conductivities σ_{f1} with these experiments is excellent, as can be seen from Fig. 2. We emphasize that the increase in the resistivity with temperature is caused only by the reduction in the density of the liquid. Our calculations show that the temperature has no noticeable effect on the electrical conductivity of the liquid below 8000 K when the density is kept constant, see Fig. 1.

The electrical conductivity of more widely expanded and hotter plasma states has also been measured.[11] However, there is only a partial overlap in the thermodynamic parameters between our results and those experiments. Furthermore, since the temperature of the molybdenum plasma could not be measured, the change in the internal energy was reported instead. The experimental uncertainties aside, we observe good agreement also with these experimental data when determining the respective temperatures with our calculated caloric equation of state.

B. Thermal conductivity

Our calculated thermal conductivities are shown in Fig. 3. The increase with the density is similar to what is observed also for the electrical conductivity in both the fluid and the solid phase. The temperature dependence in the fluid is strong and substantially nonlinear. In the solid its influence is much weaker and more difficult to resolve, especially between 1000 K and 3000 K, due to the statistical fluctuations in our results. For temperatures above about 3000 K the thermal conductivity undoubtedly rises with the temperature.

It is experimentally known[1,14] that the thermal conductivity decreases with the temperature below 1000 K, the lowest temperature for which we have produced results. By combining our calculated results with the experimental thermal conductivities below 1000 K,[14] we are able to give a very reasonable analytical fit for the thermal conductivity of solid molybdenum. Keeping in mind that the thermal conductivity naturally has a linear intrinsic temperature dependence, we choose a functional form that is analogous to Eq. (5):

$$\lambda_s = a_0 + a_1\varrho + a_2 T + a_3 \ln T \qquad (8)$$

The respective coefficients a_i are given in Table II as well. The fit curves are displayed in Fig. 3. The shallow minimum in the thermal conductivity is located close to 2000 K.

Experiments at ambient pressure[12–17] showed that the thermal conductivity decreases with the temperature up to the melting temperature. This decrease is pronounced below 1000 K[14] but weakens at higher temperature. We

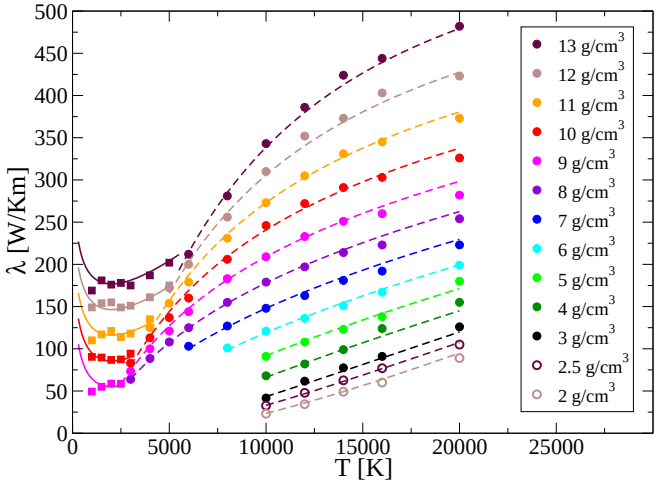

FIG. 3. (Color online) Isochores of the thermal conductivity of molybdenum. For the fluid phase the calculated values are shown as circles, whereas squares of identical color indicate values in the solid phase. The solid lines are results of Eq. (8). The dashed lines correspond to Eq. (9) for the fluid phase, respectively.

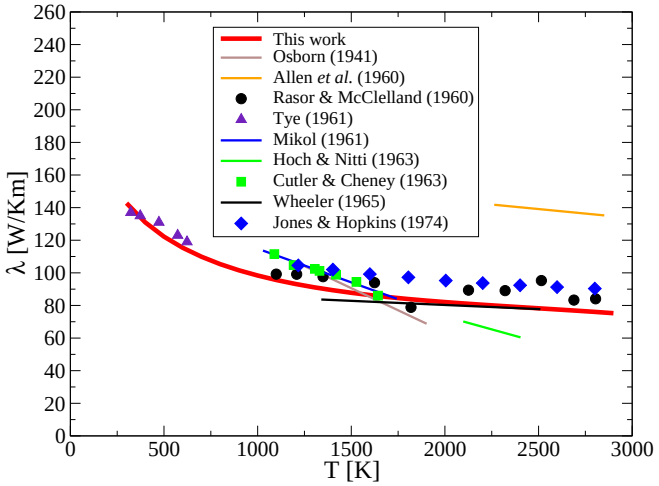

FIG. 4. (Color online) Comparison of our results for the thermal conductivity of solid molybdenum from Eq. (8) with experimental data.[12–17] The values of Mikol and Hoch & Nitti were extracted from the paper of Jones & Hopkins.[17] The experiments were performed at ambient pressure. The respective volume expansion was calculated as described in the Appendix A.

compare our fit, Eq. (8), with these experiments in Fig. 4, taking into account the thermal expansion in the experiments (see Appendix A). Given the variation between all the sets of different experiments, we can infer that the theoretical results are of high fidelity. This is especially true for the slope at high temperature, which is determined by the interplay between the nonlinearities in expansion and thermal conductivity itself.

It is particularly worth noting that the effect of thermal expansion leads to a qualitatively different temperature dependence. For example, the minimum in the thermal conductivity near 2000 K at constant density does not exist at all when the pressure is held constant instead.

TABLE IV. Coefficients for the thermal conductivity λ_f of fluid molybdenum. All units are chosen in a way that entering temperatures in K and densities in g/cm^3 leads to results in W/Km.

c_0	-7.021
c_1	1.208
c_2	0.7929
c_3	-22780
c_4	21070
c_5	-2926
c_6	1.241
c_7	-0.1914
c_8	-0.05672

For the fluid phase the thermal conductivities are fit to the following expression:

$$\ln\lambda_f = c_0 + c_1\ln\varrho + c_2\varrho + \frac{c_3}{T} + c_4\frac{\ln\varrho}{T} + c_5\frac{\varrho}{T} + c_6\ln T + c_7\ln\varrho\ln T + c_8\varrho\ln T \quad (9)$$

This functional form is a good compromise between simplicity and numerical accuracy. The nine coefficients c_i are given in Table IV and the resulting curves are included in Fig. 3.

We are not aware of experimental measurements of thermal conductivities for fluid molybdenum. If such experiments are achieved in the future, it will be very interesting to compare them to our predictions.

C. Lorenz number

Having calculated both the electrical and thermal conductivity, it is insightful to examine the Lorenz number,

$$L = \frac{e^2\lambda}{k_B^2 T\sigma}. \quad (10)$$

In regions of high electron degeneracy this quantity takes the constant value of $L = \pi^2/3$, which is known as the Wiedemann-Franz law.[19] To explore how well this relation actually holds, we plot the Lorenz number calculated by our fit formulae, Eq. (5) and (8) for the solid and Eq. (6), (7) and (9) for the fluid in Fig. 5.

The left panel of Fig. 5 shows the very systematic behavior of the isochores of the Lorenz number in the solid phase. Starting with slightly higher values than $\pi^2/3$ at room temperature, it decreases to a density-dependent minimum value and then rises again. The maximum deviation from the Wiedemann-Franz law does not exceed 10% by very much in the entire region of interest.

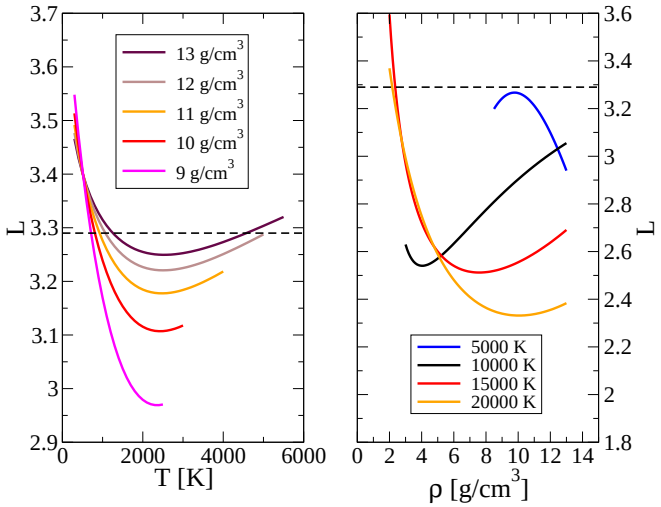

FIG. 5. (Color online) Left panel: Isochores of the Lorenz number in the solid phase. Right panel: Isotherms of the Lorenz number in the liquid phase. The dashed line indicates the Wiedemann-Franz law in both panels.

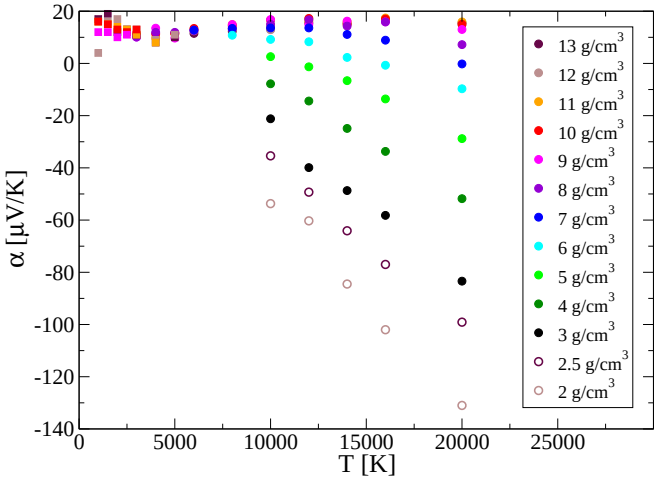

FIG. 6. (Color online) Isochores of the thermopower of molybdenum. For the fluid phase the calculated values are shown as circles, whereas squares of identical color indicate results in the solid phase.

In the fluid phase, the Lorenz number shows a much more nonlinear behavior, which is shown in the right panel of Fig. 5 along several isotherms. The deviations from the Wiedemann-Franz law are particularly strong at high temperatures, which is expected due to a decreasing electron degeneracy. There is also a particularly strong trend of a steeply rising Lorenz number toward low densities. Such behavior was already observed in earlier calculations for hydrogen,[23] where a strong increase up to one order of magnitude was observed in the partially denenerate, expanded plasma.

We find that, although the Wiedemann-Franz law is approximately valid for solid and liquid molybdenum, it is not to be relied upon in the low-density or high-temperature fluid regimes.

D. Thermopower

The thermopower is, like the Lorenz number, a very sensitive quantity, strongly influenced by the electronic structure. For electronic conductors it usually has a negative sign although exceptions are not uncommon, especially among the transition metals.[3] This is also the case for molybdenum.

We display our calculated values for the thermopower in Fig. 6. For densities between 8 and 13 g/cm^3 the thermopower takes a small and relatively constant value of about +15 μV/K. This number is the same for both the solid and the liquid so that, in contrast to the electrical and thermal conductivity, the thermopower has no noticeable discontinuity at the melting line. In the hot fluid the thermopower decreases with temperature and volume to reach large negative values.

Since the thermopower of fluid molybdenum is only of minor importance for practical applications, we did not attempt to write analytical expressions with optimized parameters for it.

Experimental data for the thermopower of molybdenum are very scarce and only avaliable for the solid up to a fairly low temperature of about 700 K.[3] Our main set of results for the transport coefficients begins at 1000 K because of the significant numerical challenges in going to lower temperatures. Achieving a converged limit ($\omega \to 0$) in the evaluation of the expressions shown in section II becomes very demanding for low-temperature metallic solids. The mathematical structure of Eq. (4), however, which is a quotient of two Onsager coefficients, helps to compensate these difficulties somewhat. Table I shows that the thermopower indeed converges much easier with the particle number than the conductivities do in the solid phase. With two additional sets of calculations, in which we used 200 ionic configurations each, we were able to calculate a well-converged thermopower for 500 K and 750 K at the experimental density. Our theoretical results are compared to the experiment[3] in Fig. 7, with very good agreement. As noted above, we predict that the thermopower levels off and remains at a value close to 15 μV/K for higher temperatures.

E. Behavior at higher temperatures

We now present an outlook on how the behavior of the electronic transport coefficients calculated in the previous sections changes at even higher temperature, i.e., up to 50 000 K. Fig. 8 shows the electrical and thermal conductivity, Lorenz number, and thermopower for the 10 g/cm^3 isochore, which roughly corresponds to the normal solid density of molybdenum.

We see that the linear decrease in the electrical conduc-

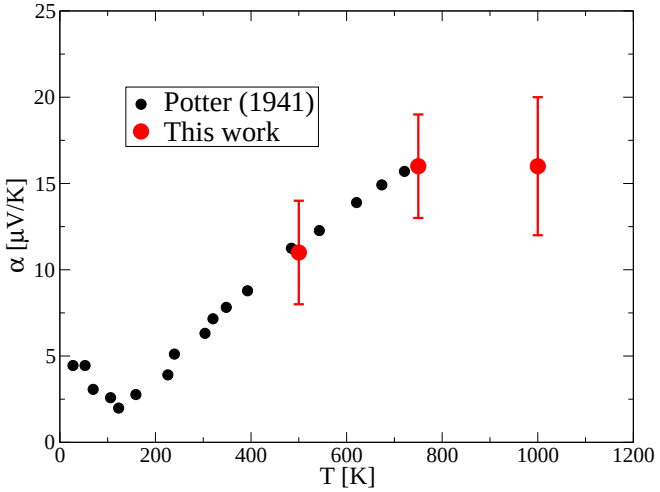

FIG. 7. (Color online) Thermopower of solid molybdenum in comparison with experimental data.[3]

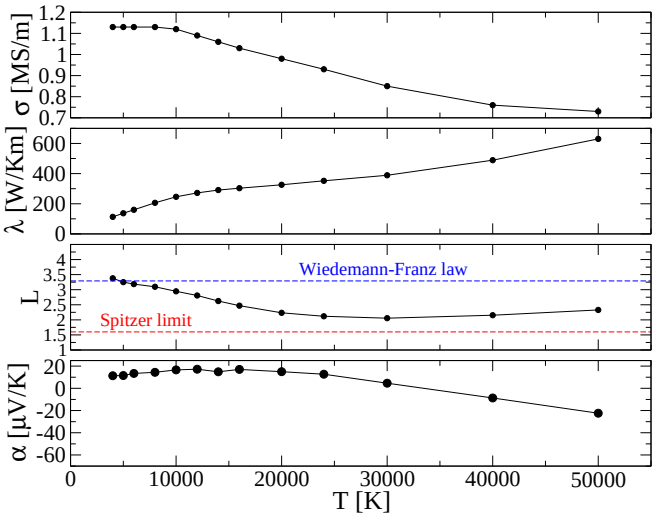

FIG. 8. (Color online) Transport properties of fluid molybdenum at 10 g/cm^3 and high temperatures.

tivity between 10 000 K and 30 000 K becomes weaker at higher temperature. The thermal conductivity shows a significant upwards bend at the same temperature. This is a characteristic sign for ionization of additional bound electrons. The Lorenz number, which decreases below 30 000 K, has a minimum there and starts rising again. One would not expect it to reach the Spitzer limit[67] at 50 000 K because the electron system remains partially degenerate there. The thermopower decreases and changes sign also near 30 000 K and takes standard negative values. This may indicate a significant decrease in the correlations within the electron system.

The nonlinear temperature behavior of the thermoelectric transport coefficients can be expected to continue up to much higher temperatures due to the high atomic number and, thus, possible ionization processes. Calculating the transport properties of dense molybdenum plasma for a wider parameter range is beyond the scope of this work. However, the results given here are certainly useful for developing, testing, or parametrizing plasma transport theories, e.g., like from Refs. 68–71 in the warm dense matter regime.

IV. SUMMARY AND DISCUSSION

We have shown that the thermoelectric transport properties of molybdenum, a refractory metal with complex electronic structure, can be calculated with high accuracy with density functional theory methods. Very good agreement with experiments of solid and liquid molybdenum is achieved for the electrical conductivity, thermal conductivity, and the thermopower. The significant influence of the density change due to thermal expansion in experiments performed at constant pressure is discussed in detail. We furthermore develop fit formulae that allow easy application of our conductivity results, valid from room temperature up to 20 000 K and a density range between 2 g/cm^3 and 13 g/cm^3. The findings are of significant importance for many practical applications of molybdenum in states of warm dense matter, especially in designing and optimizing high energy-density physics experiments, for example MAPS.[2] Furthermore, our accurate set of results can be used in the development of wide-range models for plasma transport properties that require a high fidelity also in condensed phases.

V. ACKNOWLEDGMENTS

We thank M. P. Desjarlais, K. Cochrane, L. Shulenburger, T. A. Haill, A. E. Mattsson, and D. G. Flicker for helpful discussions. This work was supported by the NNSA ASC/PEM program at Sandia. Sandia National Laboratories is a multi-program laboratory managed and operated by Sandia Corporation, a wholly owned subsidiary of Lockheed Martin Corporation, for the U.S. Department of Energys National Nuclear Security Administration under contract DE-AC04-94AL85000. (SAND2014-4396 J.) This work used the Extreme Science and Engineering Discovery Environment (XSEDE), which is supported by National Science Foundation grant number OCI-1053575. The authors acknowledge the Texas Advanced Computing Center (TACC) at The University of Texas at Austin for providing high performance computing resources that have contributed to the research results reported within this paper.

Appendix A: Thermal expansion of the solid

The independent thermodynamic quantities in our FT-DFT-MD simulations are the density and the temperature. However, experimental measurements of transport

properties in the solid are usually done at constant pressure. For direct comparisons between our theoretical and the experimental values, it is necessary to consider the thermal expansion, which becomes particularly important at high temperature.

The change in density at constant pressure can be expressed by[72]

$$\varrho(T) = \varrho_0 \exp\left[-3I(T)\right], \tag{A1}$$

where

$$\begin{aligned} I(T) = \int_{T_0}^{T} \mathrm{d}T' (&4.64 \times 10^{-6} + 6.71 \times 10^{-10} T' \\ &+ 1.24 \times 10^{-12} T'^2 - 6.43 \times 10^{-16} T'^3 \\ &+ 2.36 \times 10^{-19} T'^4). \end{aligned} \tag{A2}$$

The latter expression (temperatures to be entered in K) is a fit to experimental thermal expansivity data of molybdenum displayed in the paper of Lu *et al.*[72] and is valid from room temperature up to the melting line for ambient pressure. Whenever we process or make comparisons to experimental data in the solid phase, we employ the above expressions with a reference density of $\varrho_0 = 10.228$ g/cm^3 at $T_0 = 298$ K.[73] At the melting point (2900 K)[74] the density has reduced by about 7%.

[1] C. Agte and J. Vacek, *Wolfram und Molybdän* (Akademie, Berlin, 1959).
[2] C. S. Alexander, J. R. Asay, and T. A. Haill, J. Appl. Phys. **108**, 126101 (2010).
[3] H. H. Potter, Proc. Phys. Soc. **53**, 695 (1941).
[4] R. D. Allen, L. F. Glasier, and P. L. Jordan, J. Appl. Phys. **31**, 1382 (1960).
[5] T. R. Mattsson, N. Sandberg, R. Armiento, and A. E. Mattsson, Phys. Rev. B **80**, 224104 (2009).
[6] P. D. Desai, T. K. Chu, H. M. James, and C. Y. Ho, J. Phys. Chem. Ref. Data **13**, 1069 (1984).
[7] U. Seydel, W. Fucke, and H. Wadle, *Die Bestimmung thermophysikalischer Daten flüssiger hochschmelzender Metalle mit schnellen Pulsaufheizexperimenten* (Mannhold, Düsseldorf, 1980).
[8] G. Pottlacher, E. Kaschnitz, and H. Jäger, J. Phys.: Condens. Matter **3**, 5783 (1991).
[9] R. S. Hixson and M. A. Winkler, Int. J. Thermophys. **13**, 477 (1992).
[10] T. Hüpf, C. Cagran, G. Lohöfer, and G. Pottlacher, J. Phys. Conf. Ser. **98**, 062002 (2008).
[11] A. W. DeSilva and G. B. Vunni, Phys. Rev. E **83**, 037402 (2011).
[12] R. H. Osborn, J. O. S. A. **31**, 428 (1941).
[13] N. S. Rasor and J. D. McClelland, J. Phys. Chem. Solids **15**, 17 (1960).
[14] R. P. Tye, J. Less Common Met. **3**, 13 (1961).
[15] M. Cutler and G. T. Cheney, J. Appl. Phys. **34**, 1714 (1963).
[16] M. J. Wheeler, Brit. J. Appl. Phys. **16**, 365 (1965).
[17] M. Jones and M. R. Hopkins, phys. stat. sol. (a) **21**, 507 (1974).
[18] A. Gladun, C. Gladun, and H. Vinzelberg, phys. stat. sol. (a) **58**, 409 (1980).
[19] G. Wiedemann and R. Franz, Ann. Phys. **165**, 497 (1853).
[20] P. Hohenberg and W. Kohn, Phys. Rev. **136**, B864 (1964).
[21] W. Kohn and L. J. Sham, Phys. Rev. **140**, A1133 (1965).
[22] N. D. Mermin, Phys. Rev. **137**, A1441 (1965).
[23] B. Holst, M. French, and R. Redmer, Phys. Rev. B **83**, 235120 (2011).
[24] R. S. Hixson, D. A. Boness, J. W. Shaner, and J. A. Moriarty, Phys. Rev. Lett. **62**, 637 (1989).
[25] Y. K. Vohra and A. L. Ruoff, Phys. Rev. B **42**, 8651 (1990).
[26] R. S. Hixson and J. N. Fritz, J. Appl. Phys. **71**, 1721 (1992).
[27] D. Errandonea, B. Schwager, R. Ditz, C. Gessmann, R. Boehler, and M. Ross, Phys. Rev. B **63**, 132104 (2001).
[28] D. Santamara-Prez, M. Ross, D. Errandonea, G. D. Mukherjee, M. Mezouar, and R. Boehler, J. Chem. Phys. **130**, 124509 (2009).
[29] A. B. Belonoshko, S. I. Simak, A. E. Kochetov, B. Johansson, L. Burakovsky, and D. L. Preston, Phys. Rev. Lett. **92**, 195701 (2004).
[30] C. Cazorla, M. J. Gillan, S. Taioli, and D. Alfè, J. Chem. Phys. **126**, 194502 (2007).
[31] A. B. Belonoshko, L. Burakovsky, S. P. Chen, B. Johansson, A. S. Mikhaylushkin, D. L. Preston, S. I. Simak, and D. C. Swift, Phys. Rev. Lett. **100**, 135701 (2008).
[32] C. Cazorla, M. J. Gillan, S. Taioli, and D. Alfè, J. Phys. Conf. Ser. **121**, 012009 (2008).
[33] C. Cazorla, D. Alfè, and M. J. Gillan, Phys. Rev. B **85**, 064113 (2012).
[34] Z.-Y. Zeng, C.-E. Hu, X.-R. Chen, X.-L. Zhang, L.-C. Cai, and F.-Q. Jing, Phys. Chem. Chem. Phys. **13**, 1669 (2011).
[35] J. A. Moriarty, R. Q. Hood, and L. H. Yang, Phys. Rev. Lett. **108**, 036401 (2012).
[36] M. P. Desjarlais, Phys. Rev. B **68**, 064204 (2003).
[37] V. Recoules and J.-P. Crocombette, Phys. Rev. B **72**, 104202 (2005).
[38] T. R. Mattsson and M. P. Desjarlais, Phys. Rev. Lett. **97**, 017801 (2006).
[39] M. French, T. R. Mattsson, and R. Redmer, Phys. Rev. B **82**, 174108 (2010).
[40] D. Alfè, M. Pozzo, and M. P. Desjarlais, Phys. Rev. B **85**, 024102 (2012).
[41] J. Clérouin, P. Noiret, P. Blottiau, V. Recoules, B. Siberchicot, P. Renaudin, C. Blancard, G. Faussurier, B. Holst, and C. E. Starrett, Phys. Plasmas **19**, 082702 (2013).
[42] G. Kresse and J. Hafner, Phys. Rev. B **47**, 558 (1993).
[43] G. Kresse and J. Hafner, Phys. Rev. B **48**, 13115 (1993).
[44] G. Kresse and J. Hafner, Phys. Rev. B **49**, 14251 (1994).

[45] G. Kresse and J. Furthmüller, Phys. Rev. B **54**, 11169 (1996).
[46] J. Hafner, J. Comput. Chem. **29**, 2044 (2008).
[47] The matrix elements are extracted out of the OPTIC file. It has to be ensured that all Bloch states are considered as initial and final.
[48] R. Kubo, J. Phys. Soc. Jpn. **12**, 570 (1957).
[49] D. A. Greenwood, Proc. Phys. Soc. **71**, 585 (1958).
[50] R. Armiento and A. E. Mattsson, Phys. Rev. B **72**, 085108 (2005).
[51] A. E. Mattsson, R. Armiento, J. Paier, G. Kresse, J. M. Wills, and T. R. Mattsson, J. Chem. Phys. **128**, 084714 (2008).
[52] J. P. Perdew, K. Burke, and M. Ernzerhof, Phys. Rev. Lett. **77**, 3865 (1996).
[53] It was very challenging to converge AM05 calculations at low densities, in fact some calculations did not converge.
[54] T. R. Mattsson, S. Root, A. E. Mattsson, L. Shulenburger, R. J. Magyar, and D. G. Flicker, Phys. Rev. B, submitted(2014).
[55] P. E. Blöchl, Phys. Rev. B **50**, 17953 (1994).
[56] G. Kresse and D. Joubert, Phys. Rev. B **59**, 1758 (1999).
[57] A. E. Mattsson, *Sandia National Laboratories Report No. SAND201415971*, Tech. Rep. (Sandia National Laboratories, 2014).
[58] A. E. Mattsson, P. A. Schultz, M. P. Desjarlais, T. R. Mattsson, and K. Leung, Modell. Simul. Mater. Sci. Eng. **13**, R1 (2005).
[59] S. Nosé, J. Chem. Phys. **81**, 511 (1984).
[60] A. Baldereschi, Phys. Rev. B **7**, 5212 (1973).
[61] H. J. Monkhorst and J. D. Pack, Phys. Rev. B **13**, 5188 (1976).
[62] G. Leibfried and E. Schlömann, Nachr. Akad. Wiss. Göttingen Math.-Phys. Kl. **2**, 71 (1954).
[63] G. R. Gathers, Rep. Prog. Phys. **49**, 341 (1986).
[64] A. N. Emelyanov, A. A. Pyalling, and V. Y. Ternovoi, Int. J. Thermophys. **26**, 1985 (2005).
[65] M. French and T. R. Mattsson, J. Appl. Phys. **116**, 013510 (2014).
[66] T. E. Faber, *Introduction To The Theory Of Liquid Metals* (Cambridge University Press, Cambridge, 1972).
[67] R. Redmer, Phys. Rep. **282**, 35 (1997).
[68] Y. T. Lee and R. M. More, Phys. Fluids **27**, 1273 (1984).
[69] H. Kitamura and S. Ichimaru, Phys. Rev. E **51**, 6004 (1995).
[70] M. P. Desjarlais, Contrib. Plasma Phys. **41**, 267 (2001).
[71] S. Kuhlbrodt, B. Holst, and R. Redmer, Contrib. Plasma Phys. **45**, 73 (2005).
[72] X.-G. Lu, M. Selleby, and B. Sundman, Acta Mater. **53**, 2259 (2005).
[73] K. D. Litasov, P. I. Dorogokupets, E. Ohtani, Y. Fei, A. Shatskiy, I. S. Sharygin, P. N. Gavryushkin, S. V. Rashchenko, Y. V. Seryotkin, Y. Higo, K. Funakoshi, A. D. Chanyshev, and S. S. Lobanov, J. Appl. Phys. **113**, 093507 (2013).
[74] P. D. Desai, J. Phys. Chem. Ref. Data **16**, 91 (1987).